Received November 2, 2020, accepted November 14, 2020, date of publication November 20, 2020,
date of current version December 8, 2020.

Digital Object Identifier 10.1109/ACCESS.2020.3039527

Adaptive Transform Learning and Joint Sparsity Based PLORAKS Parallel Magnetic Resonance Image Reconstruction

JIZHONG DUAN[1,2], CHANG LIU[1,2], YU LIU[3], (Member, IEEE), AND ZHENHONG SHANG[2,4]

[1]Faculty of Information Engineering and Automation, Kunming University of Science and Technology, Kunming 650500, China
[2]Computer Technology Application Key Laboratory of Yunnan Province, Kunming University of Science and Technology, Kunming 650500, China
[3]School of Microelectronics, Tianjin University, Tianjin 300072, China
[4]Yunnan Key Laboratory of Artificial Intelligence, Kunming University of Science and Technology, Kunming 650500, China

Corresponding author: Jizhong Duan (duanjz@kust.edu.cn)

This work was supported in part by the National Natural Science Foundation of China under Grant 61861023 and Grant 12063002, in part by the Yunnan Key Research Program under Grant 2018IB007, in part by the Scientific Research Foundation of Kunming University of Science and Technology under Grant KKSY201703017, and in part by the Yunnan Provincial Major Science and Technology Special Plan Projects under Grant 202002AD080001.

ABSTRACT Parallel magnetic resonance (MR) imaging is an important acceleration technique based on the spatial sensitivities of array receivers. The recently proposed Parallel low-rank modeling of local k-space neighborhoods (PLORAKS) approach uses the low-rank matrix model based on local neighborhoods of undersampled multichannel k-space data for reconstruction purposes. The joint total variation (JTV) regularization term was then combined with the PLORAKS model to improve the quality of reconstructed images. To further improve the quality of parallel MR imaging, we propose combining adaptive transform learning and joint sparsity with the PLORAKS model to obtain two algorithms, and reconstruction problems are solved by using the alternating direction method of multipliers (ADMM) and conjugate gradient techniques. The experimental results show that the two proposed algorithms can achieve higher performance than the PLORAKS algorithm and the PLORAKS-JTV algorithm with the JTV regularization term in terms of the signal-to-noise ratio (SNR), normalized root mean square error (NRMSE), high-frequency error norm (HFEN), and structural similarity index measure (SSIM).

INDEX TERMS Parallel magnetic resonance imaging (MRI), parallel low-rank modeling of local k-space neighborhoods (PLORAKS), transform learning, alternating direction method of multipliers (ADMM).

I. INTRODUCTION

Magnetic resonance (MR) imaging is an important imaging tool for modern medical diagnoses because it has no ionizing radiation and can provide good contrast between different soft tissues. However, the scanning speed of MR imaging is fundamentally limited due to physical and physiological constraints. Increasing the scanning speed of MR imaging has been a research hotspot in recent years. Reducing the amount of acquired data is a commonly used method to accelerate MR imaging. Therefore, it is very important to reconstruct a high-quality MR image from the undersampled data. According to the emerging compressed sensing (CS) theory [1], [2], if the signal is sparse in some transform domains, it can likely be accurately reconstructed the signal from highly undersampled observation data by using nonlinear optimization methods. Since MR images are sparse in some transform domains, such as wavelet transforms and spatial finite differences, they can be reconstructed from highly undersampled k-space data according to CS theory [3]. Some CS-based MR image reconstruction methods have been proposed. The authors in [3]–[6] proposed using the composite regularization terms of ℓ_1 norms of wavelet coefficients and total variation (TV) to improve the reconstruction quality of the MR images. The authors in [7], [8] proposed using the patch-based directional wavelets (PBDW, PBDWS) to improve the quality of reconstructed MR images. The authors in [9] proposed integrating a novel iterative feature refinement (IFR) module with CS to restore meaningful structures and details without introducing too much additional complexity.

The associate editor coordinating the review of this manuscript and approving it for publication was Hengyong Yu.

In addition to the above methods of fixed sparse representation, researchers have also developed reconstruction methods based on adaptive sparse representation; these include MR image reconstruction algorithms based on dictionary learning [10] and reconstruction algorithms based on sparse transform learning [11]. In dictionary learning based MR image (DLMRI) reconstruction algorithm [10], dictionary learning and reconstruction are performed simultaneously, and k-means-based singular value decomposition (K-SVD) and orthogonal matching pursuit (OMP) are used for dictionary learning and sparse coding, respectively. However, dictionary learning and sparse coding require iteration, and this results in high computational complexity. Therefore, sparse transform learning based reconstruction algorithms for MR images (TLMRI) [11]–[16] have been proposed. In these algorithms, since transform learning and sparse coding have analytical solutions, the computational complexity is reduced.

Parallel MR imaging technology is another method for accelerating MR imaging, that is often combined with compressed sensing technology to improve the quality of reconstructed images. Parallel MR imaging uses multiple coils with different spatial sensitivities to receive data [17], [18]. Some methods, such as simultaneous acquisition of spatial harmonics (SMASH) [19], and sensitivity encoding (SENSE) [20], use the sensitivity information explicitly. The authors in [21]–[24] combined the SENSE model with the TV regularization term, and improved the reconstruction quality. However, it is difficult to measure sensitivity information with high accuracy in practical applications. Small errors in sensitivity can cause artifacts to persist in a reconstructed image. Uecker *et al.* proposed an ESPIRiT model [25] that could estimate multiple sets of coil sensitivities. Duan *et al.* [26] proposed combining the ESPIRiT model with the joint TV regularization term, and effectively improved the reconstruction quality. Another class of methods utilizes the sensitivity information implicitly to avoid the difficulty of measuring or estimating sensitivity; these methods include generalized auto-calibrating partially parallel acquisitions (GRAPPA) [27], which requires only a small amount of fully sampled auto-calibration signals (ACSs) for calibration. Iterative selfconsistent parallel imaging reconstruction (SPIRiT) [28] was a GRAPPA-based auto-calibrating method, that enforced calibration consistency for every point (acquired and unacquired) on the grid. Murphy *et al.* proposed combining the SPIRiT model with the regularization terms of the joint ℓ_1 norms of wavelet coefficients, and solving the reconstruction problem by using the projection over convex sets (POCS) algorithm [29]. The authors in [30], [31] proposed combining the SPIRiT model with the joint TV regularization term, and solving reconstruction problems by using the alternating direction method of multipliers (ADMM) and the operator splitting (OS) technique, respectively.

Recently, several calibrationless parallel imaging reconstruction methods have been proposed. The calibration-free locally low-rank encouraging reconstruction (CLEAR) method [32] uses the locally low rank (LLR) matrix constraint of the image domain for reconstruction, and Saucedo *et al.* proposed improving the computational efficiency of LLR based parallel MR imaging reconstruction [33]. The authors in [34], [35] proposed using the joint sparse model of the image domain for the reconstruction process. The joint TV regularization term was used for the reconstruction process in [36]. Both simultaneous autocalibrating and k-space estimation (SAKE) [37] and PLORAKS methods [38] use the low-rank matrix model based on the local neighborhoods of undersampled multichannel k-space data. Haldar *et al.* also proposed combining the PLORAKS model with the joint TV regularization term to further improve the reconstruction quality [38]. To further improve the reconstruction accuracy of parallel MR imaging, the authors in [39] proposed learning joint-sparse codes for calibrationfree parallel MR imaging (LINDBERG) by formulating the parallel MR imaging problem as an $\ell_2 - \ell_F - \ell_{2,1}$ minimization objective.

In addition, researchers have proposed algorithms based on deep learning for parallel MR imaging and dynamic MR imaging. Specifically, Wang *et al.* proposed a dynamic MR imaging method with both k-space and spatial prior knowledge integrated via multi-supervised network training (DIMENSION) [40]; the authors in [41] exploited a residual complex convolutional neural network for fast parallel MR imaging.

In this paper, we propose two new parallel MR image reconstruction methods to further improve the quality of reconstructed parallel MR images by combining joint sparsity and adaptive transform learning with the PLORAKS model. In summary, our contributions can be summarized as follows: Since adaptive patch-based transforms can capture local image features effectively, we propose combining adaptive transform learning with the PLORAKS model to improve the quality of reconstructed parallel MR images. To make full use of the correlations between multicoil images, we propose to introduce the joint sparsity of multiple coils. And then, reconstruction problems are solved by using the ADMM and conjugate gradient (CG) techniques. Experimental results show that the proposed methods are superior to PLORAKS and PLORAKS-JTV, and these results demonstrate the effectiveness of this method in parallel MR imaging.

The structure of this paper is as follows: In Section II, we review the LORAKS and PLORAKS models. Then, we combine joint sparsity and adaptive transform learning with the PLORAKS model, and we present our algorithms (PLORAKS-TL and PLORAKS-JTL) for solving optimization problems in Section III. Simulated experimental results and analyses are provided in Section IV. Finally, Section V concludes this paper.

II. OVERVIEW OF LORAKS AND PLORAKS

The LORAKS model was a new MR image reconstruction model based on the fact that low rank matrices could be constructed from fully-sampled k-space data when the given

image had limited support or a smooth phase. The reference work [42] described three matrices: the C matrix generated from the linear dependence of the image, the S matrix, and the G matrix constructed using the smoothly varying spatial image phase. We employ the S matrix for reconstruction due to its high reconstruction quality.

The S matrix [38], [42] can be constructed by a linear operator $R_S(\cdot) : \mathbb{C}^Q \rightarrow \mathbb{R}^{2K\times 2N_R}$ that performs linear operations on k-space data $f(n_x, n_y)$ ($n_x \in [-N_X, +N_X]$, $n_y \in [-N_Y, +N_Y]$). The definition of $R_S(\cdot)$ is as follows:

$$R_S(f) = \begin{bmatrix} S_{r_+}(f) - S_{r_-}(f) & -S_{i_+}(f) + S_{i_-}(f) \\ S_{i_+}(f) + S_{i_-}(f) & S_{r_+}(f) + S_{r_-}(f) \end{bmatrix} \quad (1)$$

where $S_{r_+}, S_{r_-}, S_{i_+}$, and $S_{i_-} \in \mathbb{R}^{K\times N_R}$ are expressed as:

$$\left[S_{r_+}(f)\right]_{km} = Real\left[f\left(n_x^{(k)} - p_m, n_y^{(k)} - q_m\right)\right] \quad (2)$$

$$\left[S_{r_-}(f)\right]_{km} = Real\left[f\left(-n_x^{(k)} - p_m, -n_y^{(k)} - q_m\right)\right] \quad (3)$$

$$\left[S_{i_+}(f)\right]_{km} = Imag\left[f\left(n_x^{(k)} - p_m, n_y^{(k)} - q_m\right)\right] \quad (4)$$

$$\left[S_{i_-}(f)\right]_{km} = Imag\left[f\left(-n_x^{(k)} - p_m, -n_y^{(k)} - q_m\right)\right] \quad (5)$$

where $k = 1, \ldots, K$, $m = 1, \ldots, N_R$, and $(n_x^{(k)}, n_y^{(k)})_{k=1}^K$ represents K different k-space positions. $-N_x + R \le n_x \le N_x - R$, $-N_y + R \le n_y \le N_y - R$, R is the neighborhood radius, $\{(p_m, q_m)\}_{m=1}^{N_R}$ denotes the ordered combination of different elements in the set $\Lambda_R = \left\{(p, q) \in \mathbb{Z}^2 : p^2 + q^2 \le R^2\right\}$, and N_R denotes the cardinality of Λ_R. The structure of the operator $R_S(\cdot)$ allows $R_S^* R_S = R_S^*(R_S(\cdot))$ to form a $Q \times Q$ diagonal matrix.

The undersampled k-space data can be expressed as:

$$d = Af \quad (6)$$

where $f \in \mathbb{C}^Q$ is the fully-sampled k-space data, $d \in \mathbb{C}^M$ is the undersampled k-space data, and $A \in \mathbb{C}^{M\times Q}$ is the undersampling matrix.

The LORAKS reconstruction problem can be formulated as the following optimization problem:

$$f = \arg\min_f \|Af - d\|_2^2 + \lambda J_r(R_S(f)) \quad (7)$$

where λ represents the regularization parameter, and $J_r(X)$ is a regularization function. In reference work [42], $J_r(X)$ is defined by:

$$J_r(X) = \sum_{k>r} \sigma_k^2 = \min_{T:\ rank(T)\le r} \|X - T\|_F^2 \quad (8)$$

where $X \in \mathbb{R}^{2K\times 2N_R}$, and σ_k is the k^{th} singular value of matrix X.

PLORAKS extends the LORAKS model to parallel MR image reconstruction. In parallel MR imaging, $f_1, \ldots, f_l, \ldots, f_L \in \mathbb{C}^Q$ are fully-sampled k-space data from L different receiver coils, and $f^P = [f_1, \ldots, f_l, \ldots, f_L] \in \mathbb{C}^{LQ}$. In PLORAKS, the modified S matrix can be constructed by a linear operator $R_{PS}(\cdot) : \mathbb{C}^{LQ} \rightarrow \mathbb{R}^{2K\times 2LN_R}$, which is defined by:

$$R_{PS}(f^P) = [R_S(f_1), \ldots, R_S(f_l), \ldots, R_S(f_L)] \quad (9)$$

The PLORAKS reconstruction problem can be expressed as the following optimization problem:

$$f^P = \arg\min_{f^P} \left\|A^P f^P - d^P\right\|_2^2 + \lambda J_r\left(R_{PS}(f^P)\right) \quad (10)$$

where $d^P = [d_1, \ldots, d_l, \ldots, d_L] \in \mathbb{C}^{LM}$, and $d_l \in \mathbb{C}^M$ is the undersampled k-space data of the l^{th} coil.

Reference [38] also combined the joint TV (JTV) regularization term with the PLORAKS model, and the corresponding reconstruction problem is as follows:

$$f^P = \arg\min_{f^P} \left\|A^P f^P - d^P\right\|_2^2 + \lambda J_r\left(R_{PS}(f^P)\right) + \alpha\left\|F^{-1} f^P\right\|_{JTV} \quad (11)$$

where F represents the coil-by-coil two-dimensional Fourier transform, $\|\cdot\|_{JTV}$ represents the JTV regularization term, and α is the regularization parameter. For convenience of expression, we omit the superscript 'P' for the variables in the following description.

III. THE PROPOSED ALGORITHMS

A. PROBLEMS FORMULATION

Although the PLORAKS model combined with the JTV regularization term can effectively improve the quality of reconstructed images, there is still much room for improvement. To further improve the reconstruction quality of parallel MR imaging, this paper combines adaptive transform learning [11], [13] with the PLORAKS model and obtains the following optimization problem:

$$\min_{f,W} \|Af - d\|_2^2 + \lambda J_r(R_S(f)) + \alpha \sum_{j=1}^{Q} \left\|WP_j(F^{-1}f)\right\|_0 \quad s.t.\ W^T W = I \quad (12)$$

where $P_j(\cdot) : \mathbb{C}^{LQ} \rightarrow \mathbb{R}^{n\times L}$ is the j^{th} linear operator that extracts an image patch of size $\sqrt{n}\times\sqrt{n}$ from each coil image, and then converts these L image patches into a $\mathbb{C}^{n\times L}$ matrix. $W \in \mathbb{R}^{n\times n}$ represents an adaptive sparse transform learned from those image patches.

To make full use of the correlations between multicoil images, we propose to introduce the joint sparsity of multiple coils, and we formulate this problem as follows:

$$\min_{f,W} \|Af - d\|_2^2 + \lambda J_r(R_S(f)) + \alpha \sum_{j=1}^{Q} \left\|WP_j(F^{-1}f)\right\|_{0,2} \quad s.t.\ W^T W = I \quad (13)$$

where $\|w\|_{0,2} = \left\|\sum_{l=1}^{L} |w_l|^2\right\|_0$ is a joint ℓ_0-norm similar to the joint ℓ_1-norm [29], [43].

B. PROBLEMS SOLUTIONS

By introducing the auxiliary variables $x = F^{-1}f \in \mathbb{C}^{LQ}$ and $B_j = WP_j(x) \in \mathbb{C}^{n\times L}$, and their corresponding Lagrange multipliers ($u_x \in \mathbb{C}^{LQ}$, and $u_{B_j} \in \mathbb{C}^{n\times L}$, respectively), problem (12) can be transformed into the following subproblems

by using the ADMM method:

$$\min_{W} \frac{\mu_2}{2} \sum_{j=1}^{Q} \left\| WP_j(x) - (B_j - u_{B_j}) \right\|_2^2 s.t.\ W^T W = I \quad (14)$$

$$\min_{B} \sum_{j=1}^{Q} \left\{ \alpha \left\| B_j \right\|_0 + \frac{\mu_2}{2} \left\| B_j - WP_j(x) - u_{B_j} \right\|_2^2 \right\} \quad (15)$$

$$\min_{x} \frac{\mu_2}{2} \sum_{j=1}^{Q} \left\| WP_j(x) - (B_j - u_{B_j}) \right\|_2^2 + \frac{\mu_1}{2} \left\| x - F^{-1} f - u_x \right\|_2^2 \quad (16)$$

$$\min_{f} \|Af - d\|_2^2 + \lambda J_r\left(R_S(f)\right) + \frac{\mu_1}{2} \left\| F^{-1} f - (x - u_x) \right\|_2^2 \quad (17)$$

$$u_x = u_x + \left(F^{-1} f - x \right) \quad (18)$$

$$u_{B_j} = u_{B_j} + \left(WP_j(x) - B_j \right) \quad (19)$$

where $B \in \mathbb{C}^{n \times LQ}$ is a matrix concatenating $B_1, \ldots, B_j, \ldots, B_Q$, i.e., $B = [B_1, \ldots, B_j, \ldots, B_Q]$, and $u_B \in \mathbb{C}^{n \times LQ}$ is a matrix concatenating $u_{B_1}, \ldots, u_{B_j}, \ldots, u_{B_Q}$, i.e., $u_B = [u_{B_1}, \ldots, u_{B_j}, \ldots, u_{B_Q}]$.

Transform Update: let $X = [P_1(x), \ldots, P_j(x), \ldots, P_Q(x)] \in \mathbb{R}^{n \times LQ}$; then, problem (15) can be rewritten as:

$$\hat{W} = \arg\min_{W} \frac{\mu_2}{2} \|WX - (B - u_B)\|_2^2 \ s.t.\ W^T W = I \quad (20)$$

According to references [11], [13], if $X(B - u_B)^H$ has a full singular value decomposition (SVD) of $U \Sigma V^H$, the solution of problem (20) is given by:

$$W = VU^H \quad (21)$$

Sparse coding: problem (15) can be written as:

$$B_j = \arg\min_{B_j} \alpha \left\| B_j \right\|_0 + \frac{\mu_2}{2} \left\| B_j - WP_j(x) - u_{B_j} \right\|_2^2 \quad (22)$$

The solution of problem (22) is given by:

$$B_j = H\left(WP_j(x) + u_{B_j}, \alpha/\mu_2 \right) \quad (23)$$

where $H(x, \theta)$ denotes the hard-thresholding operator [11], which is defined as:

$$H(x, \theta) = \begin{cases} 0, & |x| < \theta \\ x, & |x| \geq \theta \end{cases} \quad (24)$$

where x and θ represent the input matrix and threshold, respectively.

When considering the joint sparsity of multiple coils, problem (22) should be modified to the following joint denoising problem:

$$B_j = \arg\min_{B_j} \alpha \left\| B_j \right\|_{0,2} + \frac{\mu_2}{2} \left\| B_j - WP_j(x) - u_{B_j} \right\|_2^2 \quad (25)$$

Problem (25) can be solved by:

$$B_j = H_J\left(WP_j(x) + u_{B_j}, \alpha/\mu_2 \right) \quad (26)$$

where $H_J(x, \theta)$ is defined as:

$$H_J(x, \theta) = \begin{cases} 0, & \sqrt{\sum_{l=1}^{L} |x_l|^2} < \theta \\ x, & \sqrt{\sum_{l=1}^{L} |x_l|^2} \geq \theta \end{cases} \quad (27)$$

Image update: Let the derivative of the objective function of (16) be zero; then, we can obtain:

$$\left(\mu_2 \sum_{j=1}^{Q} P_j^H W^H W P_j + \mu_1 I \right) x = \mu_2 \sum_{j=1}^{Q} P_j^H \left(W^H (B_j - u_{B_j}) \right) + \mu_1 \left(F^{-1} f + u_x \right) \quad (28)$$

Since $W^H W = I$ and $\sum_{j=1}^{Q} P_j^H P_j$ is a diagonal matrix, the analytical solution is given by:

$$x = \frac{\mu_2 \sum_{j=1}^{Q} P_j^H \left(W^H (B_j - u_{B_j}) \right) + \mu_1 \left(F^{-1} f + u_x \right)}{\mu_2 \sum_{j=1}^{Q} P_j^H P_j + \mu_1 I} \quad (29)$$

Reference [44] introduces a majorizer for the function $J_r(R_x(f))$ at point $\hat{f}^{i-1}$:

$$h_S\left(f, \hat{f}^{i-1} \right) \triangleq \left\| R_S(f) N_r \left(R_S\left(\hat{f}^{i-1} \right) \right) \right\|_F^2 \quad (30)$$

where $N_r(X)$ is an operator that generates a $2LN_R \times (2LN_R - r)$ matrix whose columns are equal to the right singular vector associated with the smallest $q - r$ value or zero singular value in the generalized SVD of X. Then, problem (17) can be reformulated as follows:

$$\hat{f}^i = \arg\min_{f} \|Af - d\|_2^2 + \lambda \left\| R_S(f) N_r \left(R_S\left(\hat{f}^{i-1} \right) \right) \right\|_F^2 + \frac{\mu_1}{2} \left\| F^{-1} f - (x - u_x) \right\|_2^2 \quad (31)$$

Problem (31) can be solved using the CG method.

All subproblems can be solved, so we obtain parallel MR imaging reconstruction algorithms based on transform learning and joint transform learning called: PLORAKS-TL and PLORAKS-JTL, which are summarized in Algorithm 1.

IV. SIMULATION EXPERIMENT AND ANALYSIS

A. EXPERIMENTAL SETUP

In the following experiments, we compare the PLORAKS-TL and PLORAKS-JTL algorithms with the PLORAKS (with no regularization term), and PLORAKS-JTV (with the JTV regularization term) models. All the compared algorithms are implemented using MATLAB (MathWorks, Natick, MA).

To compare the reconstruction performance of all the algorithms, we used four sets of fully-sampled in vivo human data sets, namely dataset1, dataset2, dataset3, and dataset4, as shown in Fig. 1. Dataset1 and dataset2 are human brain slices acquired by using an eight-channel head coil. Dataset3 is cine data set acquired by using a 28-channel coil,

Algorithm 1 Joint Sparsity and Transform Learning Based PLORAKS Parallel MR Imaging Reconstruction Algorithms (PLORAKS-TL and PLORAKS-JTL)

1: Set $B^1 = 0, W^1 = 0, x^1 = 0, f^1 = 0, u_x^0 = 0, u_{B_j}^1 = 0, i = 0$
2: **repeat**
3: $i = i + 1$
4: $W^{i+1} = VU^H$, $X(B^i - u_B)^H$ has the full SVD of $U\Sigma V^H$
5: ${B_j}^{i+1} = H\left(W^{i+1}P_j(x) + u_{B_j}, \alpha/\mu_2\right)$ for PLORAKS-TL
6: Or ${B_j}^{i+1} = H_J\left(W^{i+1}P_j(x) + u_{B_j}, \alpha/\mu_2\right)$ for PLORAKS-JTL
7: x^{i+1} is given by using the equation (29)
8: f^{i+1} is given by solving the problem (31) using the conjugate gradient method
9: ${u_x}^{i+1} = {u_x}^i + \left(F^{-1}f^{i+1} - x^{i+1}\right)$
10: ${u_{B_j}}^{i+1} = {u_{B_j}}^i + \left(W^{i+1}P_j(x) - {B_j}^{i+1}\right)$
11: **until** some stopping criteria met
12: Output: $f = f^{i+1}$

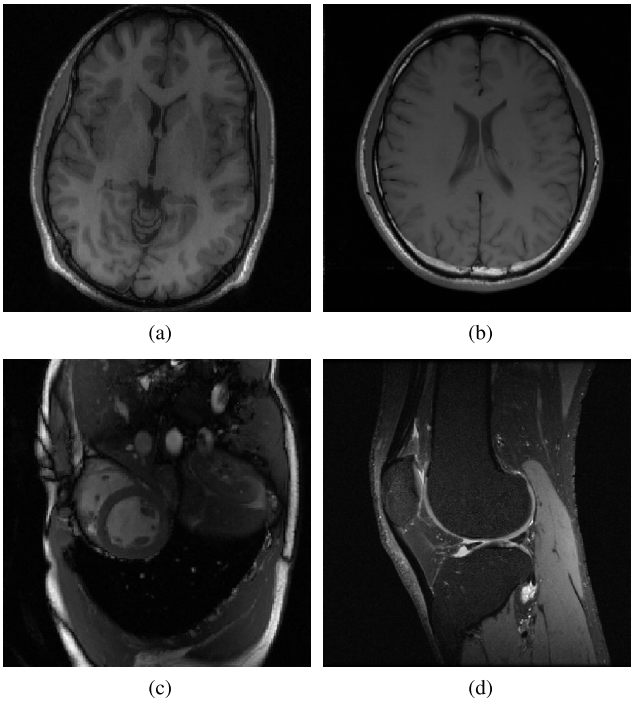

FIGURE 1. The reference images from fully sampled data sets, (a) dataset1, (b) dataset2, (c) dataset3, and (d) dataset4.

which is then compressed to 12 virtual coils. Dataset4 is a knee data set acquired by an 8-channel HD knee coil. The testing data sets are generated by retrospectively undersampling the fully-sampled data sets using the 2D Poisson-disc undersampling mask with an acceleration factor of R (excluding ACSs), as shown in Fig. 2.

All the following experiments are carried out on a laptop computer with an Intel (R) Core (TM) i5-10210U processor @ 1.6 GHz, 12 GB memory and a Windows 10 operating system (64 bit). All the parameters of the compared algorithms are tuned to achieve the optimal signal-to-noise ratio (SNR) [30] values. In the following experiments, we use the SNR, normalized root mean square error (NRMSE) [28], high-frequency error norm (HFEN) [10], and structural similarity index measure (SSIM) [45] as metrics to quantitatively evaluate the quality of reconstructed images. Higher SNR and SSIM values or lower NRMSE and HFEN values indicate better image reconstruction quality. The SNR is defined as follows:

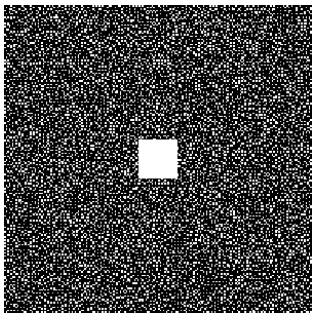

FIGURE 2. A 2D Poisson-disc undersampling mask with 4× acceleration and 24 × 24 ACSs.

$$SNR = 10\log_{10}\left(\frac{Var}{MSE}\right) \tag{32}$$

where MSE represents the mean square error between the reconstructed image $\hat{x}$ and the reference image x, Var represents the variance of x, and x and $\hat{x}$ are calculated from the fully sampled k-space data and the reconstructed k-space data, respectively by using $SoSF(f)$. $SoSF(f)$ is defined as follows:

$$x = SoSF(f) = \sqrt{\sum_{l=1}^{L}\left|(F^{-1}f)_l\right|^2} \tag{33}$$

The NRMSE is defined as follows:

$$NRMSE = \frac{\left\|\hat{x} - x\right\|_2}{\max(x) - \min(x)} \tag{34}$$

The HFEN is defined as follows:

$$HFEN = \sqrt{\frac{\left\|LoG(\hat{x}) - LoG(x)\right\|_F^2}{\|LoG(x)\|_F^2}} \tag{35}$$

where $LoG(\cdot)$ is a Laplacian Gaussian filter, which is used to capture the edges of the image, the size of the filter kernel is 15×15 pixels, and the standard deviation is 1.5 pixels.

The SSIM is defined as follows:

$$SSIM = \frac{(2u_x u_{\hat{x}} + c_1)(2\sigma_{x\hat{x}} + c_2)}{\left(u_x^2 + u_{\hat{x}}^2 + c_1\right)\left(\sigma_x^2 + \sigma_{\hat{x}}^2 + c_2\right)} \tag{36}$$

where u_x and $u_{\hat{x}}$ are the means of x and $\hat{x}$, respectively, σ_x^2 and $\sigma_{\hat{x}}^2$ are the variances of x and $\hat{x}$, respectively, and $\sigma_{x\hat{x}}$ is the covariance of $\hat{x}$ and x.

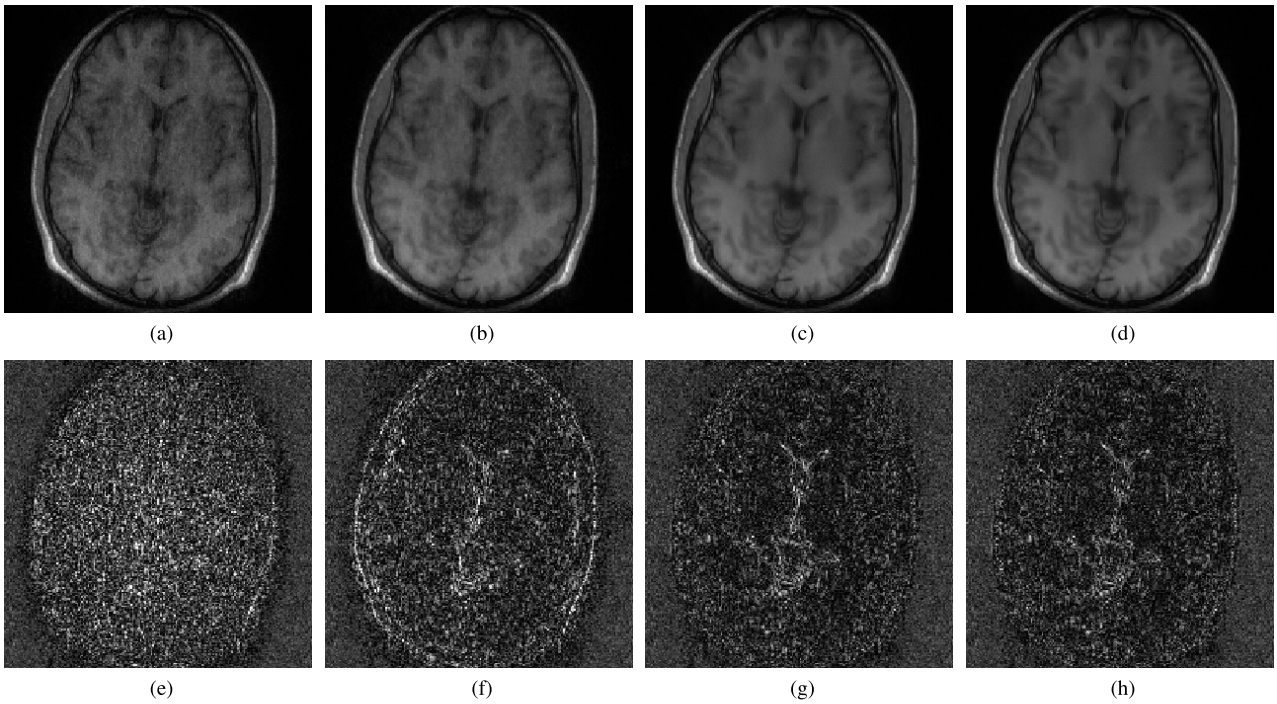

FIGURE 3. The comparison of parallel MR image reconstructions for dataset1 using the Poisson-disc undersampling with 6× acceleration and 24 × 24 ACSs. (a), (b), (c), and (d) are reconstructed by PLORAKS, PLORAKS-JTV, PLORAKS-TL, PLORAKS-JTL, respectively. (e), (f), (g), and (h) are their corresponding error maps, respectively.

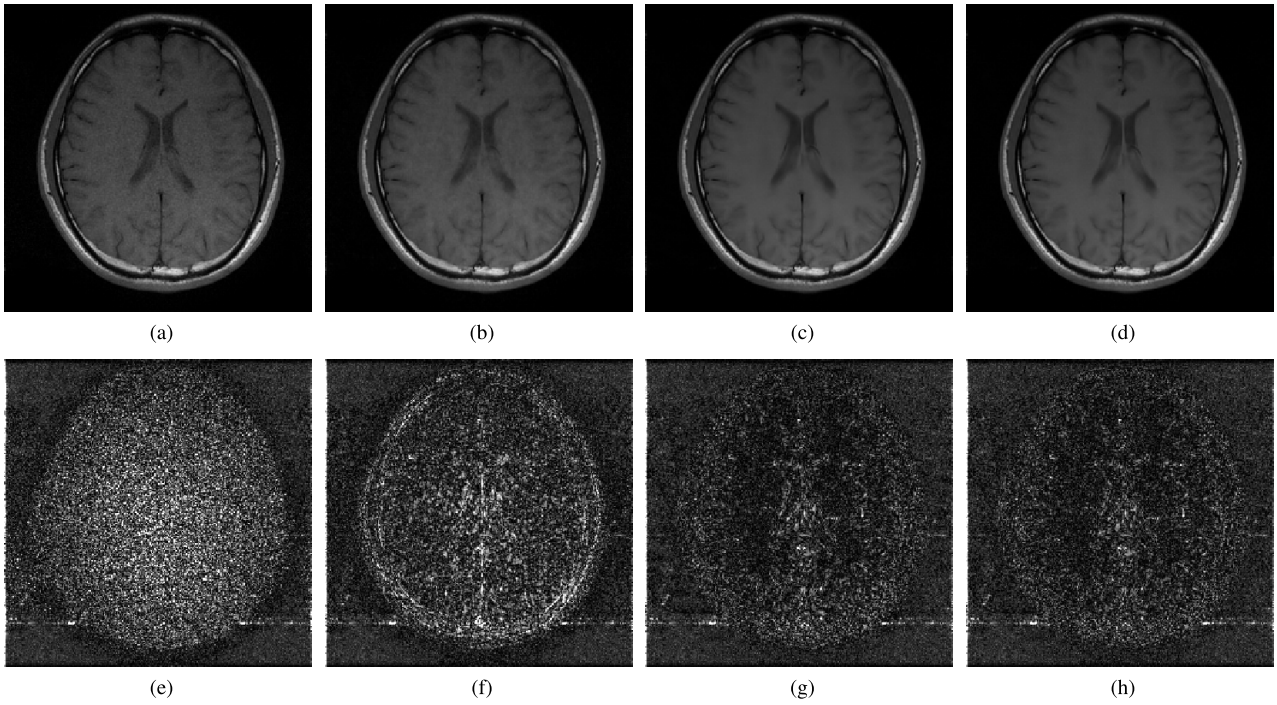

FIGURE 4. The comparison of parallel MR image reconstructions for dataset2 using the Poisson-disc undersampling with 6× acceleration and 24 × 24 ACSs. (a), (b), (c), and (d) are reconstructed by PLORAKS, PLORAKS-JTV, PLORAKS-TL, PLORAKS-JTL, respectively. (e), (f), (g), and (h) are their corresponding error maps, respectively.

B. COMPARISON OF RESULTS WITH A 2D POISSON-DISC UNDERSAMPLING SCHEME

Visual comparisons of the images reconstructed by the compared algorithms on the four data sets with an acceleration factor of 6 are shown in Figs. 3-6. As shown in Figs. 3-6, we can see that the images reconstructed by the PLORAKS method exhibit severe grainy artifacts, the PLORAKS-JTV method alleviates those artifacts but results in oversmoothed

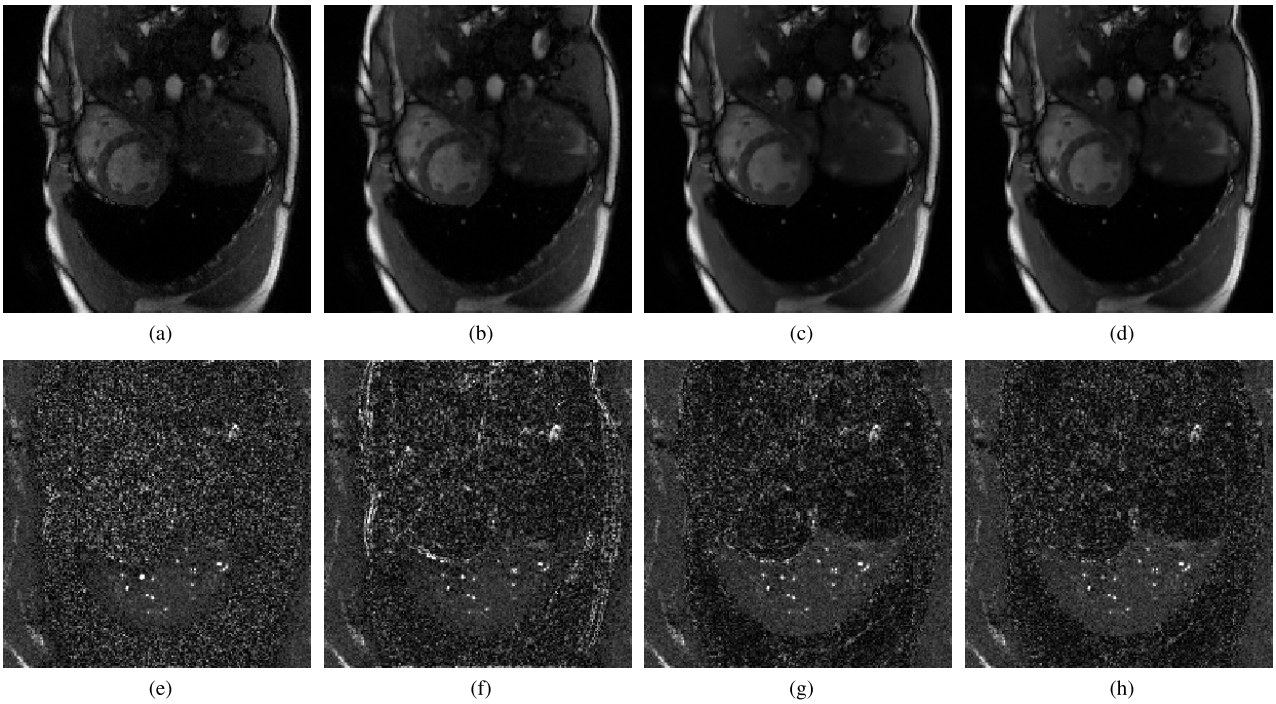

FIGURE 5. The comparison of parallel MR image reconstructions for dataset3 using the Poisson-disc undersampling with 6× acceleration and 24 × 24 ACSs. (a), (b), (c), and (d) are reconstructed by PLORAKS, PLORAKS-JTV, PLORAKS-TL, PLORAKS-JTL, respectively. (e), (f), (g), and (h) are their corresponding error maps, respectively.

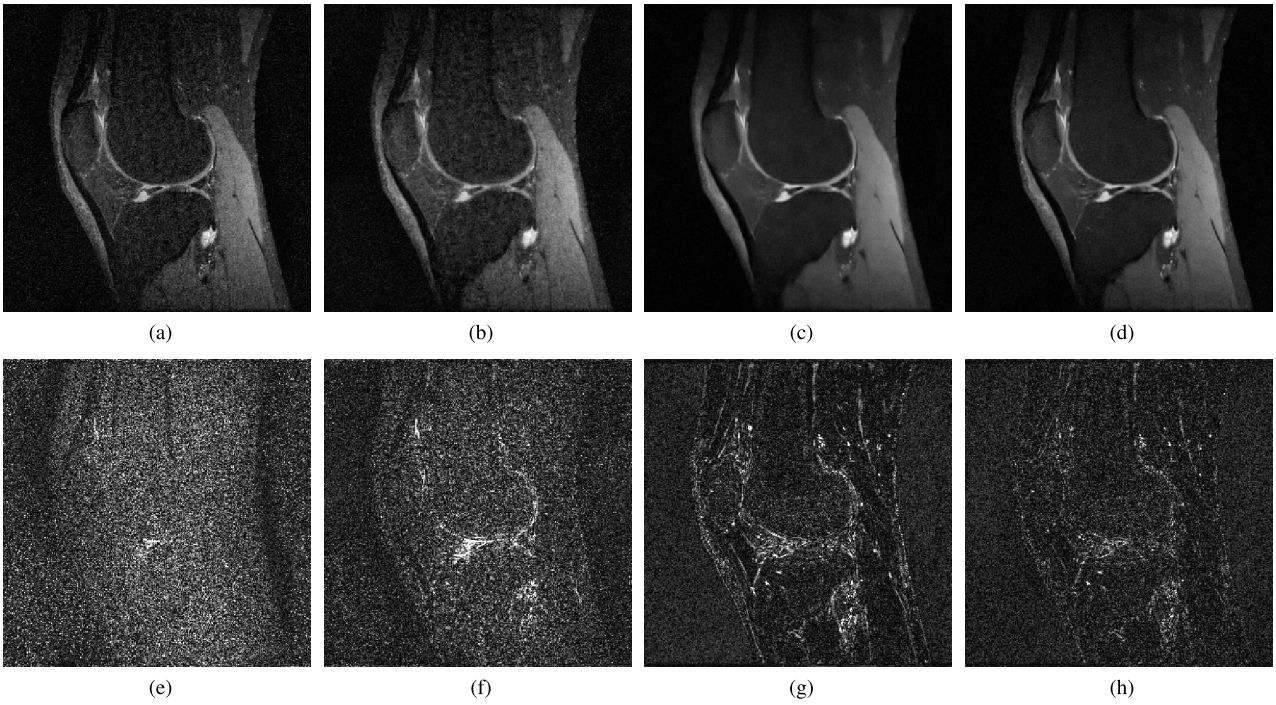

FIGURE 6. The comparison of parallel MR image reconstructions for dataset4 using the Poisson-disc undersampling with 6× acceleration and 24 × 24 ACSs. (a), (b), (c), and (d) are reconstructed by PLORAKS, PLORAKS-JTV, PLORAKS-TL, PLORAKS-JTL, respectively. (e), (f), (g), and (h) are their corresponding error maps, respectively.

edges in the reconstructed images, and the PLORAKS-TL and PLORAKS-JTL models further alleviate the artifacts and preserve the details missing in the images output by other algorithms. As shown in Fig. 6, the PLORAKS-JTL model solves the problem of oversmoothed edges observed in the image reconstructed by the PLORAKS-TL model.

We quantitatively evaluate the quality of the images reconstructed by the four compared algorithms using 2D

TABLE 1. The values of SNRs, NRMSEs, HFENs and SSIMs of the compared reconstruction algorithms for dataset1 using the Poisson-disc undersampling with different sampling ratios and 24 × 24 ACSs.

Algorihtms	Metrics	$R=3$	$R=4$	$R=5$	$R=6$	$R=7$	$R=8$
PLORAKS	SNR	20.85	18.98	17.5	16.33	15.42	14.69
	NRMSE	0.0126	0.0157	0.0186	0.0213	0.0237	0.0257
	HFEN	0.1287	0.1636	0.2226	0.2711	0.321	0.3575
	SSIM	0.9046	0.8639	0.828	0.7929	0.7677	0.7375
PLORAKS-JTV	SNR	21.54	20.07	18.64	17.76	16.36	15.4
	NRMSE	0.0117	0.0138	0.0163	0.0181	0.0212	0.0237
	HFEN	0.1141	0.1523	0.1967	0.2322	0.2903	0.3423
	SSIM	0.9165	0.8924	0.8622	0.8466	0.8022	0.7746
PLORAKS-TL	SNR	22.16	20.92	19.85	19.14	18.21	17.45
	NRMSE	0.0109	0.0125	0.0142	0.0155	0.0172	0.0187
	HFEN	0.1024	0.1267	0.1587	0.1831	0.2219	0.2584
	SSIM	0.9272	0.9073	0.8881	0.8729	0.8516	0.8311
PLORAKS-JTL	SNR	22.23	21.02	19.94	19.21	18.32	17.55
	NRMSE	0.0108	0.0124	0.014	0.0153	0.0169	0.0185
	HFEN	0.1004	0.123	0.155	0.1775	0.2146	0.2518
	SSIM	0.9283	0.9088	0.8899	0.8747	0.8546	0.8349

TABLE 2. The values of SNRs, NRMSEs, HFENs and SSIMs of the compared reconstruction algorithms for dataset2 using the Poisson-disc undersampling with different sampling ratios and 24 × 24 ACSs.

Algorihtms	Metrics	$R=3$	$R=4$	$R=5$	$R=6$	$R=7$	$R=8$
PLORAKS	SNR	27.51	25.71	23.8	21.85	20.77	19.37
	NRMSE	0.0059	0.0073	0.0091	0.0114	0.0129	0.0152
	HFEN	0.0599	0.076	0.0972	0.1262	0.1463	0.1756
	SSIM	0.962	0.9438	0.92	0.8838	0.8591	0.828
PLORAKS-JTV	SNR	28.44	26.65	25.22	23.67	22.38	21.24
	NRMSE	0.0053	0.0065	0.0077	0.0092	0.0107	0.0122
	HFEN	0.0565	0.0729	0.0925	0.1194	0.1444	0.1681
	SSIM	0.9688	0.9581	0.9486	0.9339	0.9228	0.9083
PLORAKS-TL	SNR	29.44	27.88	26.8	25.7	25.04	23.87
	NRMSE	0.0048	0.0057	0.0066	0.0073	0.0081	0.0093
	HFEN	0.047	0.0568	0.0684	0.0812	0.0884	0.0969
	SSIM	0.9739	0.9669	0.9603	0.954	0.9493	0.942
PLORAKS-JTL	SNR	29.39	27.88	26.66	25.71	25.02	24.43
	NRMSE	0.0048	0.0057	0.0066	0.0073	0.0079	0.0085
	HFEN	0.0472	0.0569	0.0684	0.08	0.0886	0.0973
	SSIM	0.9741	0.9667	0.9605	0.9544	0.9502	0.9455

Poisson-disc undersampling with different sampling ratios and 24 × 24 ACSs for dataset1-dataset4. Tables 1-4 tabulate the SNRs, NRMSEs, HFENs, and SSIMs of all the compared algorithms.

As shown in Tables 1-3, PLORAKS-JTV can achieve average SNRs that are approximately 1 dB, 1.4 dB, and 0.3 dB higher than those of PLORAKS for dataset1, dataset2, and dataset3, respectively. The PLORAKS-TL and PLORAKS-JTL models can obtain comparable average SNR values, which are approximately 1.3 dB, 1.8 dB, and 0.9 dB higher than those of the PLORAKS-JTV model, for dataset1, dataset2, and dataset3, respectively. As shown in Table 4, PLORAKS-JTV can achieve an average SNR that is approximately 1.6 dB higher than that of PLORAKS. The PLORAKS-TL model can obtain an SNR that is approximately 2.3 dB higher than that of PLORAKS-JTV. The average SNR of PLORAKS-JTL is approximately 0.9 dB

TABLE 3. The values of SNRs, NRMSEs, HFENs and SSIMs of the compared reconstruction algorithms for dataset3 using the Poisson-disc undersampling with different sampling ratios and 24 × 24 ACSs.

Algorihtms	Metrics	$R=3$	$R=4$	$R=5$	$R=6$	$R=7$	$R=8$
PLORAKS	SNR	21.38	19.66	18.33	17.2	16.06	15.32
	NRMSE	0.0122	0.0148	0.0173	0.0197	0.0225	0.0245
	HFEN	0.0765	0.0966	0.1216	0.1419	0.1759	0.1976
	SSIM	0.9223	0.8879	0.8553	0.8202	0.7862	0.7601
PLORAKS-JTV	SNR	21.57	19.94	18.83	17.52	16.43	15.7
	NRMSE	0.0119	0.0144	0.0163	0.019	0.0216	0.0234
	HFEN	0.0702	0.092	0.1123	0.1441	0.1741	0.197
	SSIM	0.9241	0.8957	0.8782	0.8556	0.8312	0.8141
PLORAKS-TL	SNR	21.86	20.38	19.38	18.63	17.91	17.33
	NRMSE	0.0115	0.0137	0.0153	0.0167	0.0182	0.0194
	HFEN	0.0667	0.0825	0.0985	0.1126	0.1266	0.1407
	SSIM	0.9334	0.9089	0.8898	0.873	0.8556	0.8406
PLORAKS-JTL	SNR	21.97	20.5	19.56	18.78	18.14	17.62
	NRMSE	0.0114	0.0135	0.015	0.0164	0.0177	0.0188
	HFEN	0.0671	0.0828	0.0971	0.1125	0.1243	0.1365
	SSIM	0.9342	0.9103	0.8922	0.8745	0.8589	0.8462

TABLE 4. The values of SNRs, NRMSEs, HFENs and SSIMs of the compared reconstruction algorithms for dataset4 using the Poisson-disc undersampling with different sampling ratios and 24 × 24 ACSs.

Algorihtms	Metrics	$R=3$	$R=4$	$R=5$	$R=6$	$R=7$	$R=8$
PLORAKS	SNR	14.06	11.63	10.32	9.23	8.58	8.23
	NRMSE	0.0249	0.033	0.0384	0.0435	0.0469	0.0488
	HFEN	0.3244	0.4456	0.5177	0.5883	0.6415	0.6872
	SSIM	0.6846	0.5765	0.4981	0.4372	0.4042	0.3822
PLORAKS-JTV	SNR	14.9	12.71	12.18	11.09	10.58	9.97
	NRMSE	0.0226	0.0291	0.031	0.0351	0.0372	0.04
	HFEN	0.3333	0.4572	0.4984	0.58	0.6519	0.6885
	SSIM	0.7036	0.6051	0.5711	0.5171	0.4916	0.4669
PLORAKS-TL	SNR	16.65	15.14	14.17	13.6	13.12	12.53
	NRMSE	0.0185	0.022	0.0246	0.0263	0.0278	0.0297
	HFEN	0.2466	0.3247	0.3733	0.4144	0.4472	0.4949
	SSIM	0.8029	0.7494	0.7219	0.7023	0.6821	0.663
PLORAKS-JTL	SNR	17.23	15.99	15.14	14.64	14.12	13.62
	NRMSE	0.0173	0.02	0.022	0.0233	0.0248	0.0262
	HFEN	0.2198	0.2657	0.2912	0.3256	0.3484	0.3805
	SSIM	0.8056	0.7619	0.7367	0.7206	0.6993	0.6831

higher than that of PLORAKS-TL. Overall, introducing an additional regularization term contributes to improving the quality of the image reconstructed by PLORAKS. The PLORAKS-JTL algorithm always achieves the best performance in terms of the SNRs, NRMSEs, HFENs, and SSIMs among the compared algorithms.

C. ALGORITHMIC PERFORMANCE COMPARISON WITH DIFFERENT ACS SIZES

In addition, PLORAKS is a calibration-less parallel image reconstruction method that does not require ACSs [38]. We also compare PLORAKS and PLORAKS-JTL with a coil-by-coil auto-calibrating reconstruction method using the joint TV regularization term (SPIRiT-JTV) [31] from the undersampled k-space data with an acceleration factor of 3 and different ACS sizes. As shown in Table 5, SPIRiT-JTV can achieve an SNR of 21.24 dB when the size of the ACSs

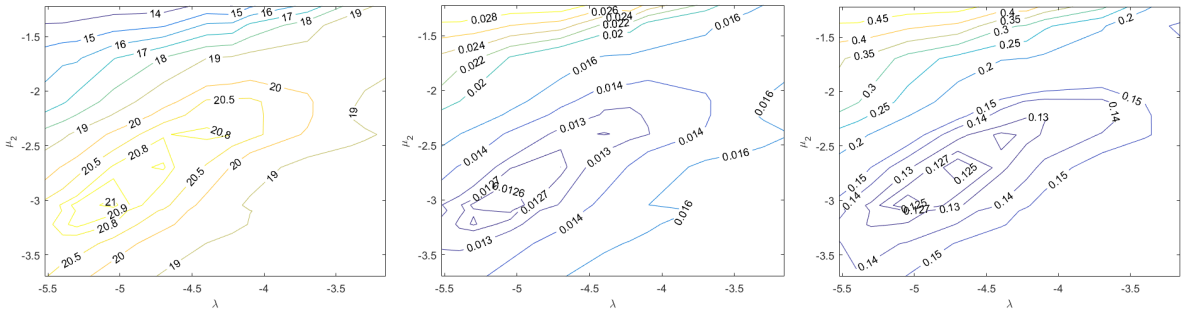

FIGURE 7. Contour plots show the values of (a) SNR, (b) NRMSE and (c) HFEN versus λ and μ_2 when reconstructing dataset1 using the Poisson-disc undersampling with 4× acceleration and 24 × 24 ACSs.

TABLE 5. SNRs, NRMSEs, HFENs and SSIMs of the compared reconstruction algorithms for the dataset1 from the Poisson-disc undersampling with different sampling ratios and 24 × 24 ACSs.

Algorithms	Size of ACS				
	24×24	12×12	8×8	4×4	0×0
SPIRiT-JTV	21.24	19.19	10.04	-	-
PLORAKS	20.85	20.49	20.19	19.67	17.52
PLORAKS-JTL	22.23	21.86	21.69	20.97	20.77

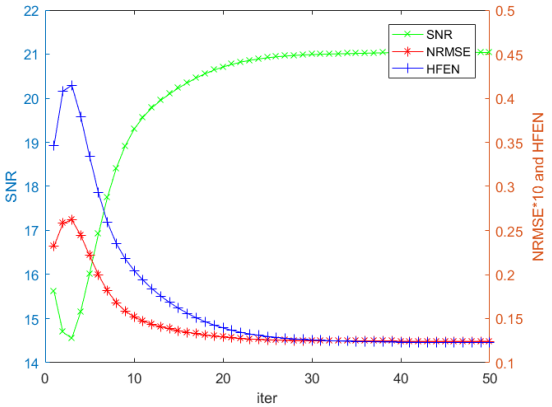

FIGURE 8. The values of the SNR, NRMSE and HFEN versus the number of iterations when reconstructing dataset1 using the 2D Poisson-disc undersampling with 4× acceleration and 24 × 24 ACSs.

is 24 × 24; when the size of the ACSs is reduced to 12 × 12, the SNR value decreases by approximately 2 dB; and the SNR value dramatically decreases to 10.04 dB when the ACSs is 8 × 8. Therefore, we do not perform reconstruction experiments for the 4 × 4 and 0 × 0 ACS sizes. For the PLORAKS algorithm, when the size of the ACSs gradually reduced from 24×24 to 0×0, the SNR of reconstructed image decreases from 20.85 dB to 17.52 dB, with a reduction of only 3.33 dB. PLORAKS-JTL can effectively improve the quality of images reconstructed by PLORAKS and reduce the impact of the size of the ACSs on the reconstruction performance. Specifically, when the size of the ACSs decreases from 24×24 to 0×0, the SNR of the reconstructed image decreases from 22.23 dB to 20.77 dB, with a reduction of only 1.46 dB.

In general, the SPIRiT-JTV method depends heavily on the size of the ACSs. When the size of the ACSs gradually decreases from 24 × 24 to 0 × 0, the SNR of the image

TABLE 6. Comparison of run time of the compared reconstruction algorithms for the dataset1 from the 2D Poisson-disc undersampling with 6× acceleration and 24 × 24 ACSs.

Algorithms	Run Time (s)
PLORAKS	76
PLORAKS-JTV	293
PLORAKS-TL	544
PLORAKS-JTL	616

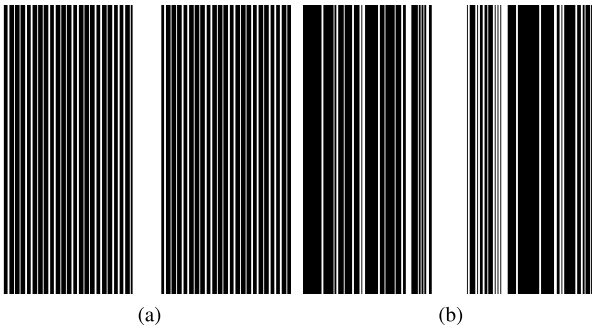

FIGURE 9. 1D undersampling masks with 3× acceleration and 20 ACS lines. (a) 1D uniform undersampling, (b) 1D random undersampling.

reconstructed by PLORAKS decreases by 3.33 dB, while the SNR of the image reconstructed by PLORAKS-JTL reduces by only 1.46 dB. PLORAKS-JTL is insensitive to the size of the ACSs.

D. SENSITIVITY TO PARAMETER SETTINGS

In this subsection, we discuss the sensitivity of the proposed algorithm's parameters by adjusting one parameter and fixing the others. The regularization parameter α exists in the form of α/μ_2 in our method, and we set α as 2×10^{-7}. We have found that β and μ_1 are insensitive to reconstruction accuracy, so we set β as 10^{-4} and μ_1 as 10^{-4}. We then evaluate the proposed algorithm on dataset1 with a 2D Poisson sampling mask with 4× acceleration and 24 × 24 ACSs using different parameter sets, i.e., $\mu_2 \in [10^{-4}, 10^{-1}]$ and $\lambda \in [10^{-6}, 10^{-3}]$, logarithmically spaced. Contour plots show the values of the SNR, NRMSE and HFEN versus λ and μ_2 when reconstructing dataset1 from the Poisson-disc undersampling with 4× acceleration and 24 × 24 ACSs, as shown in Fig. 7. We choose λ and μ_2 that maximize the SNR and minimize the NRMSE and HFEN, respectively. The optimal $\lambda = 10^{-5}$ and the optimal $\mu_2 = 10^{-3}$; and these values are roughly consistent for all three metrics (SNR, NRMSE and HFEN).

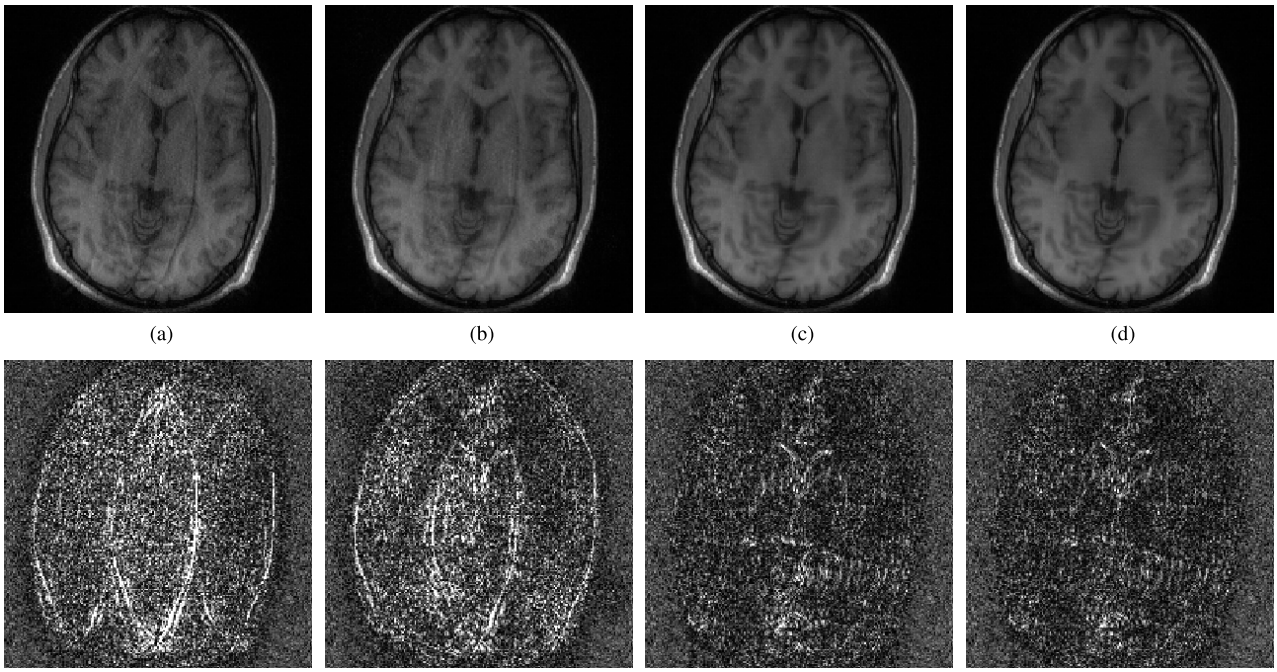

FIGURE 10. The comparison of parallel MR image reconstructions for dataset1 using the 1D uniform undersampling with 3× acceleration and 20 ACS lines. (a), (b), (c), and (d) are reconstructed by PLORAKS, PLORAKS-JTV, PLORAKS-TL, PLORAKS-JTL, respectively. (e), (f), (g), and (h) are their corresponding error maps, respectively.

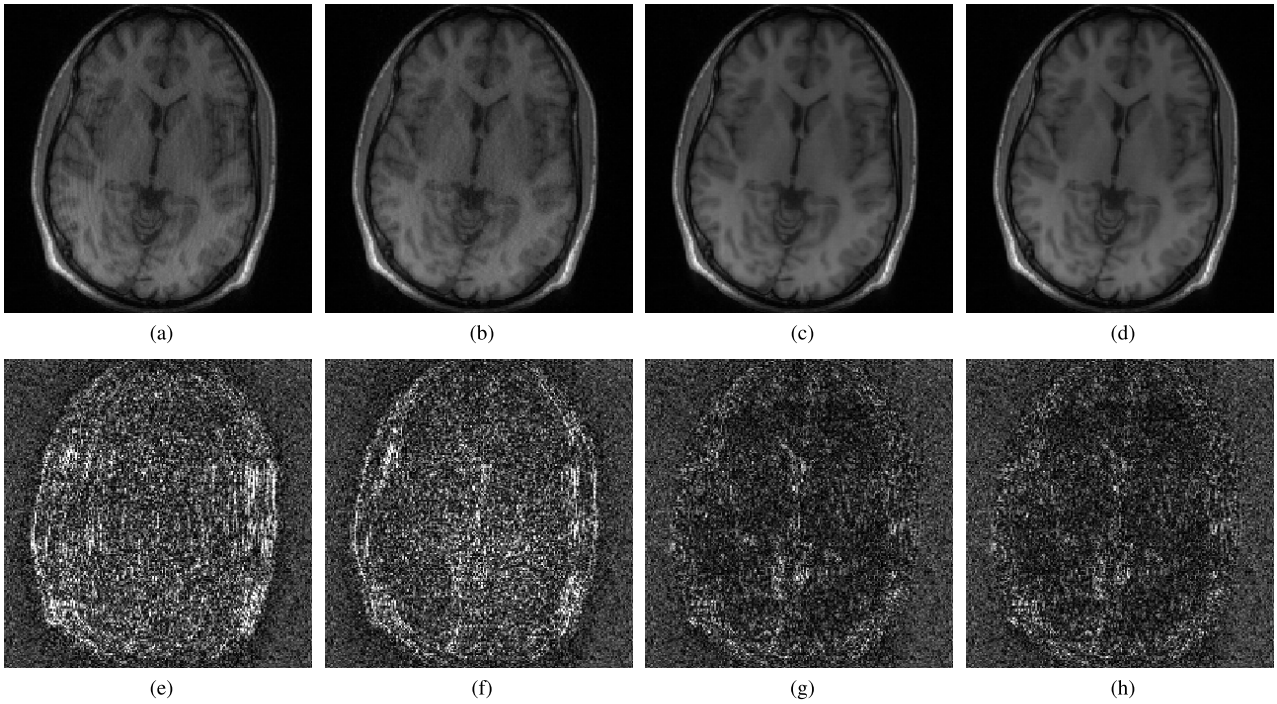

FIGURE 11. The comparison of parallel MR image reconstructions for dataset1 using the 1D random undersampling with 3× acceleration and 20 ACS lines. (a), (b), (c), and (d) are reconstructed by PLORAKS, PLORAKS-JTV, PLORAKS-TL, PLORAKS-JTL, respectively. (e), (f), (g), and (h) are their corresponding error maps, respectively.

E. CONVERGENCE PROPERTY

To reflect the convergence property of the proposed method (PLORAKS-JTL), we explore the development of three metrics (SNR, NRMSE and HFEN) with respect to the number of iterations. Fig. 8 illustrates the values of the SNR, NRMSE and HFEN versus the number of iterations when reconstructing dataset1 from the 2D Poisson-disc undersampling with 4× acceleration and 24 × 24 ACSs. As shown in Fig. 8, all three metrics achieved approximate convergence after 30 iterations.

F. COMPARISON OF RUN TIME

We also compare the run time of PLORAKS, PLORAKS-JTV, PLORAKS-TL, and PLORAKS-JTL. Table 6 tabulates the run time of all the compared algorithms for parallel MR reconstructions from the 2D Poisson-disc undersampling with 6× acceleration and 24 × 24 ACSs for the dataset1. As shown in Table 6, the PLORAKS-JTL method is the slowest among the compared algorithms. The run time of PLORAKS-JTL is $K_{out} \times (K_{CG} \times T_{CG} + T_{JTL})$, where K_{out} is the number of outer iterations, K_{CG} is the number of CG iterations, T_{CG} is the run time of one CG iteration, and T_{JTL} is the run time of one JTL denoising iteration. In the future, we will try our best to solve problem (13) more efficiently, and we will optimize the algorithm by using the graphics processing unit (GPU) to greatly reduce the run time of each JTL denoising iteration.

G. COMPARISON RESULTS WITH A 1D UNDERSAMPLING SCHEME

We also compare the MR image reconstructions for dataset1 from a 1D uniform undersampling and 1D random undersampling with 3× acceleration and 20 ACS lines, as shown in Fig. 9. The visual comparisons are shown in Figs. 10-11. As shown in Figs. 10-11, we can see that PLORAKS-TL and PLORAKS-JTL greatly improve the imaging accuracy and reduce the artifacts exhibited in the images output by other algorithms, and PLORAKS-JTL has slightly better imaging quality than PLORAKS-TL.

V. CONCLUSION

In this paper, we propose two algorithms that combine joint sparsity and adaptive sparsifying transform learning with the PLORAKS model to improve the reconstruction quality of parallel MR imaging, and the reconstruction problems are solved by using the ADMM and conjugate gradient techniques. The experimental results show that the two proposed algorithms can achieve higher performance than the PLORAKS algorithm and the PLORAKS-JTV algorithm with the joint TV regularization term in terms of their SNR, NRMSE, HFEN, and SSIM values. In addition, the proposed algorithms are insensitive to the size of the ACSs.

ACKNOWLEDGMENT

The authors would like to thank D. Weller, S. Ravishankar, B. Wen, J. P. Haldar, L. Ying, M. Lustig, M. Uecker, and J. F. M. Schmidt for sharing their code and/or in vivo data sets. The authors would also like to thank the editors and anonymous reviewers for their helpful comments and suggestions for this manuscript.

REFERENCES

[1] E. J. Candes, J. Romberg, and T. Tao, "Robust uncertainty principles: Exact signal reconstruction from highly incomplete frequency information," *IEEE Trans. Inf. Theory*, vol. 52, no. 2, pp. 489–509, Feb. 2006.

[2] D. L. Donoho, "For most large underdetermined systems of linear equations the minimal ℓ_1-norm solution is also the sparsest solution," *Commun. Pure Appl. Math.*, vol. 59, no. 6, pp. 797–829, 2006.

[3] M. Lustig, D. Donoho, and J. M. Pauly, "Sparse MRI: The application of compressed sensing for rapid MR imaging," *Magn. Reson. Med.*, vol. 58, no. 6, pp. 1182–1195, Dec. 2007.

[4] J. Duan, Y. Liu, and L. Zhang, "Bregman iteration based efficient algorithm for MR image reconstruction from undersampled K-space data," *IEEE Signal Process. Lett.*, vol. 20, no. 8, pp. 831–834, Aug. 2013.

[5] J. Yang, Y. Zhang, and W. Yin, "A fast alternating direction method for TVL1-L2 signal reconstruction from partial Fourier data," *IEEE J. Sel. Topics Signal Process.*, vol. 4, no. 2, pp. 288–297, Apr. 2010.

[6] J. Huang, S. Zhang, H. Li, and D. Metaxas, "Composite splitting algorithms for convex optimization," *Comput. Vis. Image Understand.*, vol. 115, no. 12, pp. 1610–1622, Dec. 2011.

[7] B. Ning, X. Qu, D. Guo, C. Hu, and Z. Chen, "Magnetic resonance image reconstruction using trained geometric directions in 2D redundant wavelets domain and non-convex optimization," *Magn. Reson. Imag.*, vol. 31, no. 9, pp. 1611–1622, Nov. 2013.

[8] X. Qu, D. Guo, B. Ning, Y. Hou, Y. Lin, S. Cai, and Z. Chen, "Undersampled MRI reconstruction with patch-based directional wavelets," *Magn. Reson. Imag.*, vol. 30, no. 7, pp. 964–977, Sep. 2012.

[9] S. Wang, J. Liu, Q. Liu, L. Ying, X. Liu, H. Zheng, and D. Liang, "Iterative feature refinement for accurate undersampled MR image reconstruction," *Phys. Med. Biol.*, vol. 61, no. 9, pp. 3291–3316, May 2016.

[10] S. Ravishankar and Y. Bresler, "MR image reconstruction from highly undersampled k-space data by dictionary learning," *IEEE Trans. Med. Imag.*, vol. 30, no. 5, pp. 1028–1041, May 2011.

[11] S. Ravishankar and Y. Bresler, "Sparsifying transform learning with efficient optimal updates and convergence guarantees," *IEEE Trans. Signal Process.*, vol. 63, no. 9, pp. 2389–2404, May 2015.

[12] S. Ravishankar and Y. Bresler, "Learning doubly sparse transforms for images," *IEEE Trans. Image Process.*, vol. 22, no. 12, pp. 4598–4612, Dec. 2013.

[13] S. Ravishankar and Y. Bresler, "Efficient blind compressed sensing using sparsifying transforms with convergence guarantees and application to magnetic resonance imaging," *SIAM J. Imag. Sci.*, vol. 8, no. 4, pp. 2519–2557, Jan. 2015.

[14] S. Ravishankar and Y. Bresler, "Data-driven learning of a union of sparsifying transforms model for blind compressed sensing," *IEEE Trans. Comput. Imag.*, vol. 2, no. 3, pp. 294–309, Sep. 2016.

[15] Z. Zhan, J.-F. Cai, D. Guo, Y. Liu, Z. Chen, and X. Qu, "Fast multiclass dictionaries learning with geometrical directions in MRI reconstruction," *IEEE Trans. Biomed. Eng.*, vol. 63, no. 9, pp. 1850–1861, Sep. 2016.

[16] B. Wen, S. Ravishankar, and Y. Bresler, "FRIST–flipping and rotation invariant sparsifying transform learning and applications," *Inverse Problems*, vol. 33, no. 7, Jul. 2017, Art. no. 074007.

[17] K. P. Pruessmann, "Encoding and reconstruction in parallel MRI," *NMR Biomed.*, vol. 19, no. 3, pp. 288–299, 2006.

[18] K. P. Pruessmann, M. Weiger, P. Börnert, and P. Boesiger, "Advances in sensitivity encoding with arbitraryk-space trajectories," *Magn. Reson. Med.*, vol. 46, no. 4, pp. 638–651, Oct. 2001.

[19] D. K. Sodickson and W. J. Manning, "Simultaneous acquisition of spatial harmonics (SMASH): Fast imaging with radiofrequency coil arrays," *Magn. Reson. Med.*, vol. 38, no. 4, pp. 591–603, Oct. 1997.

[20] K. P. Pruessmann, M. Weiger, M. B. Scheidegger, and P. Boesiger, "SENSE: Sensitivity encoding for fast MRI," *Magn. Reson. Med.*, vol. 42, no. 5, pp. 952–962, Nov. 1999.

[21] D. Liang, B. Liu, J. Wang, and L. Ying, "Accelerating SENSE using compressed sensing," *Magn. Reson. Med.*, vol. 62, no. 6, pp. 1574–1584, Dec. 2009.

[22] S. Ramani and J. A. Fessler, "Parallel MR image reconstruction using augmented lagrangian methods," *IEEE Trans. Med. Imag.*, vol. 30, no. 3, pp. 694–706, Mar. 2011.

[23] X. Ye, Y. Chen, and F. Huang, "Computational acceleration for MR image reconstruction in partially parallel imaging," *IEEE Trans. Med. Imag.*, vol. 30, no. 5, pp. 1055–1063, May 2011.

[24] M. J. Muckley, D. C. Noll, and J. A. Fessler, "Fast parallel MR image reconstruction via B1-based, adaptive restart, iterative soft thresholding algorithms (BARISTA)," *IEEE Trans. Med. Imag.*, vol. 34, no. 2, pp. 578–588, Feb. 2015.

[25] M. Uecker, P. Lai, M. J. Murphy, P. Virtue, M. Elad, J. M. Pauly, S. S. Vasanawala, and M. Lustig, "ESPIRiT–An eigenvalue approach to autocalibrating parallel MRI: Where SENSE meets GRAPPA," *Magn. Reson. Med.*, vol. 71, no. 3, pp. 990–1001, Mar. 2014.

[26] J. Duan, Z. Bao, and Y. Liu, "Eigenvector-based SPIRiT parallel MR imaging reconstruction based on lp pseudo-norm joint total variation," *Magn. Reson. Imag.*, vol. 58, pp. 108–115, May 2019.

[27] M. A. Griswold, P. M. Jakob, R. M. Heidemann, M. Nittka, V. Jellus, J. Wang, B. Kiefer, and A. Haase, "Generalized autocalibrating partially parallel acquisitions (GRAPPA)," *Magn. Reson. Med.*, vol. 47, no. 6, pp. 1202–1210, Jun. 2002.
[28] M. Lustig and J. M. Pauly, "SPIRiT: Iterative self-consistent parallel imaging reconstruction from arbitrary k-space," *Magn. Reson. Med.*, vol. 64, no. 2, pp. 457–471, Aug. 2010.
[29] M. Murphy, M. Alley, J. Demmel, K. Keutzer, S. Vasanawala, and M. Lustig, "Fast ℓ_1-SPIRiT compressed sensing parallel imaging MRI: Scalable parallel implementation and clinically feasible runtime," *IEEE Trans. Med. Imag.*, vol. 31, no. 6, pp. 1250–1262, Jun. 2012.
[30] J. Duan, Y. Liu, and P. Jing, "Efficient operator splitting algorithm for joint sparsity-regularized SPIRiT-based parallel MR imaging reconstruction," *Magn. Reson. Imag.*, vol. 46, pp. 81–89, Feb. 2018.
[31] D. S. Weller, S. Ramani, and J. A. Fessler, "Augmented lagrangian with variable splitting for faster non-Cartesian L_1-SPIRiT MR image reconstruction," *IEEE Trans. Med. Imag.*, vol. 33, no. 2, pp. 351–361, Feb. 2014.
[32] J. D. Trzasko and A. Manduca, "Calibrationless parallel MRI using CLEAR," in *Proc. Conf. Rec. Forty 5th Asilomar Conf. Signals, Syst. Comput. (ASILOMAR)*, Nov. 2011, pp. 75–79.
[33] A. Saucedo, S. Lefkimmiatis, N. Rangwala, and K. Sung, "Improved computational efficiency of locally low rank MRI reconstruction using iterative random patch adjustments," *IEEE Trans. Med. Imag.*, vol. 36, no. 6, pp. 1209–1220, Jun. 2017.
[34] A. Majumdar and R. K. Ward, "Calibration-less multi-coil MR image reconstruction," *Magn. Reson. Imag.*, vol. 30, no. 7, pp. 1032–1045, Sep. 2012.
[35] A. Majumdar, K. N. Chaudhury, and R. Ward, "Calibrationless parallel magnetic resonance imaging: A joint sparsity model," *Sensors*, vol. 13, no. 12, pp. 16714–16735, 2013.
[36] C. Chen, Y. Li, and J. Huang, "Calibrationless parallel MRI with joint total variation regularization," in *Proc. Med. Image Comput. Comput.-Assisted Intervent (MICCAI)*, vol. 8151, Nagoya, Japan, 2013, pp. 106–114.
[37] P. J. Shin, P. E. Z. Larson, M. A. Ohliger, M. Elad, J. M. Pauly, D. B. Vigneron, and M. Lustig, "Calibrationless parallel imaging reconstruction based on structured low-rank matrix completion," *Magn. Reson. Med.*, vol. 72, no. 4, pp. 959–970, Oct. 2014.
[38] J. P. Haldar and J. Zhuo, "P-LORAKS: Low-rank modeling of local k-space neighborhoods with parallel imaging data," *Magn. Reson. Med.*, vol. 75, no. 4, pp. 1499–1514, Apr. 2016.
[39] S. Wang, S. Tan, Y. Gao, Q. Liu, L. Ying, T. Xiao, Y. Liu, X. Liu, H. Zheng, and D. Liang, "Learning joint-sparse codes for calibration-free parallel MR imaging," *IEEE Trans. Med. Imag.*, vol. 37, no. 1, pp. 251–261, Jan. 2018.
[40] S. Wang, Z. Ke, H. Cheng, S. Jia, L. Ying, H. Zheng, and D. Liang, "DIMENSION: Dynamic MR imaging with both k-space and spatial prior knowledge obtained via multi-supervised network training," *NMR Biomed.*, no. e4131, Sep. 2019, doi: 10.1002/nbm.4131.
[41] S. Wang, H. Cheng, L. Ying, T. Xiao, Z. Ke, H. Zheng, and D. Liang, "DeepcomplexMRI: Exploiting deep residual network for fast parallel MR imaging with complex convolution," *Magn. Reson. Imag.*, vol. 68, pp. 136–147, May 2020.
[42] J. P. Haldar, "Low-rank modeling of local k-space neighborhoods (LORAKS) for constrained MRI," *IEEE Trans. Med. Imag.*, vol. 33, no. 3, pp. 668–681, Mar. 2014.
[43] S. S. Vasanawala, M. T. Alley, B. A. Hargreaves, R. A. Barth, J. M. Pauly, and M. Lustig, "Improved pediatric MR imaging with compressed sensing," *Radiology*, vol. 256, no. 2, pp. 607–616, Aug. 2010.
[44] T. H. Kim, K. Setsompop, and J. P. Haldar, "LORAKS makes better SENSE: Phase-constrained partial Fourier SENSE reconstruction without phase calibration," *Magn. Reson. Med.*, vol. 77, no. 3, pp. 1021–1035, Mar. 2017.
[45] Z. Wang, A. C. Bovik, H. R. Sheikh, and E. P. Simoncelli, "Image quality assessment: From error visibility to structural similarity," *IEEE Trans. Image Process.*, vol. 13, no. 4, pp. 600–612, Apr. 2004.

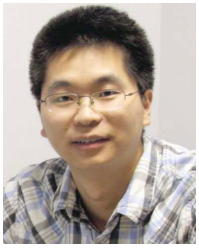

JIZHONG DUAN received the B.E. degree in communication engineering, the M.S. degree in signal and information processing, and the Ph.D. degree in information and communication engineering from Tianjin University, Tianjin, China, in 2007, 2009, and 2013, respectively.

He was a Visiting Scholar with the Department of Computer Science and Engineering, Lehigh University, Bethlehem, PA, USA, from 2011 to 2012. He is currently an Associate Professor with the Faculty of Information Engineering and Automation and the Computer Technology Application Key Laboratory of Yunnan Province, Kunming University of Science and Technology, Kunming, China. His research interests include medical image processing, compressed sensing, and magnetic resonance imaging.

CHANG LIU received the B.E. degree from the College of Internet of Things Engineering, Hohai University, in 2018. He is currently pursuing the M.E. degree with the Faculty of Information Engineering and Automation, Kunming University of Science and Technology, Kunming, China. His research interests include image processing, compressed sensing, and magnetic resonance imaging.

YU LIU (Member, IEEE) received the B.Eng. degree in electronic engineering, the M.Eng. degree in information and communication engineering, and the Ph.D. degree in signal and information processing from Tianjin University, Tianjin, China, in 1998, 2002, and 2005, respectively.

He was an Electronic Engineer with Nantian Electronics Information Corporation, Shenzhen, China, from 1998 to 2000. From 2011 to 2012, he was a Visiting Fellow with the Department of Electrical Engineering, Princeton University, Princeton, NJ, USA. Since 2017, he has been a Professor with the School of Microelectronics, Tianjin University. His research interests include signal/video processing, medical signal processing, multimedia systems, compressed sensing, and indoor positioning systems.

ZHENHONG SHANG received the B.S. degree from the Department of Electronic Science and Engineering, Nankai University, Tianjin, China, in 1998, the M.S. degree in computer science from the Kunming University of Science and Technology, Kunming, China, in 2001, and the Ph.D. degree in computer science from the Beijing Institute of Technology, Beijing, China, in 2004. He is currently an Associate Professor with the Kunming University of Science and Technology. His current research interests include sparse signal representation and image processing.